Supporting Information for

Monitoring the Interannual Spatiotemporal Changes in the Land Surface Thermal Environment in both Urban and Rural Regions from 2003 to 2013 in China Based on Remote Sensing

Yuanzheng Li,[1,2,3] Lan Wang,[4] Liping Zhang,[5] and Qing Wang,[6]

[1] School of Resources and Environment, Henan University of Economics and Law, Zhengzhou 450046, China.
[2] Academician Laboratory for Urban and Rural Spatial Data Mining of Henan Province, Henan University of Economics and Law, Zhengzhou 450046, China.
[3] State Key Laboratory of Urban and Regional Ecology, Research Center for Eco-Environmental Sciences, Chinese Academy of Sciences, Beijing 100085, China.
[4] Key Laboratory of Urban Environment and Health, Institute of Urban Environment, Chinese Academy of Sciences, Xiamen 361021, China.
[5] Center for Environmental Zoning, Chinese Academy for Environmental Planning, Ministry of Environmental Protection of China, Beijing 100012, China.
[6] Guangdong Key Laboratory of Sugarcane Improvement and Biorefinery, Guangdong Provincial Bioengineering Institute (Guangzhou Sugarcane Industry Research Institute), Guangzhou, China.

Correspondence should be addressed to Lan Wang; wlsunshinelz@163.com

Supporting figures

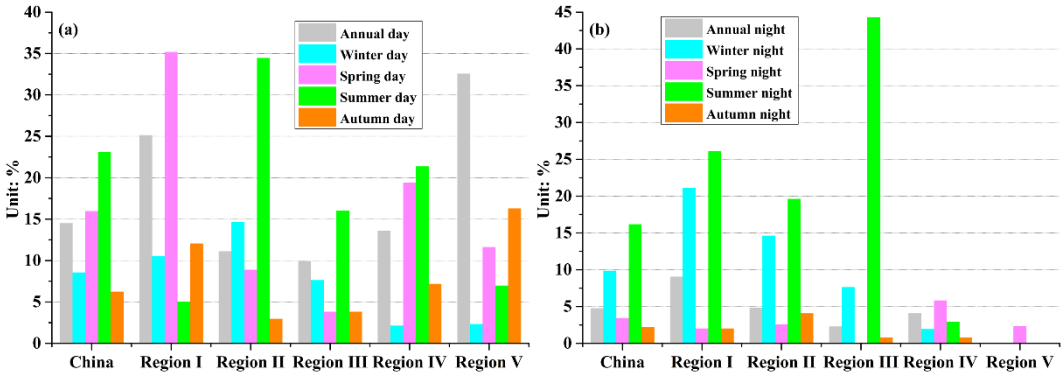

Figure S1. The percentages of reference rural regions whose annual and seasonal variation rates of mean LSTs significantly changed during both the daytime and night-time from 2003 to 2013 in the five environmental regions of China.

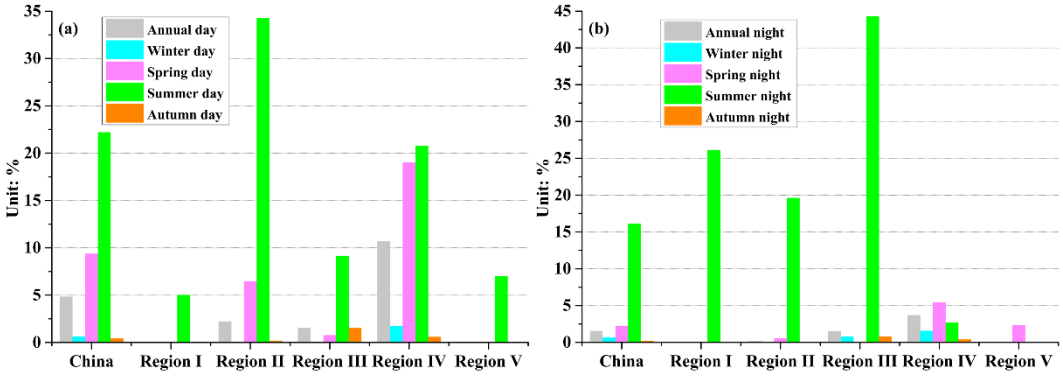

Figure S2. The percentages of reference rural regions whose annual and seasonal variation rates of mean LSTs significantly positively changed during both the daytime and night-time from 2003 to 2013 in the five environmental regions of China.

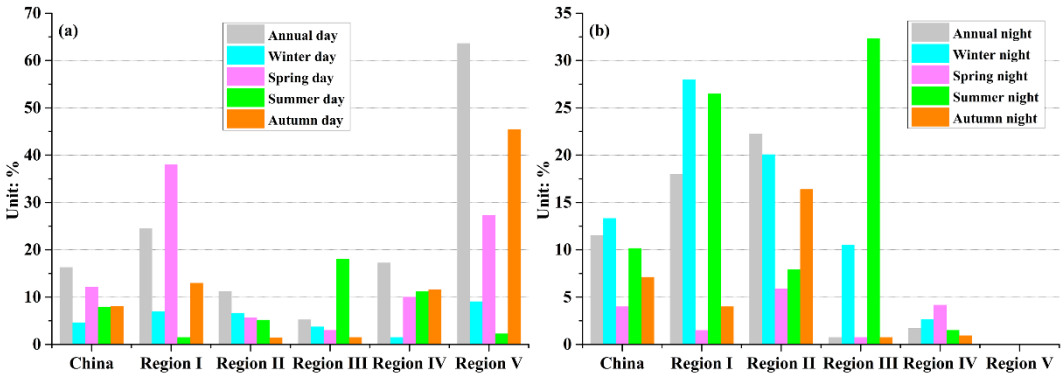

Figure S3. The percentages of urban regions whose annual and seasonal variation rates of mean LSTs significantly changed during both the daytime and night-time from 2003 to 2013 in the five environmental regions of China.

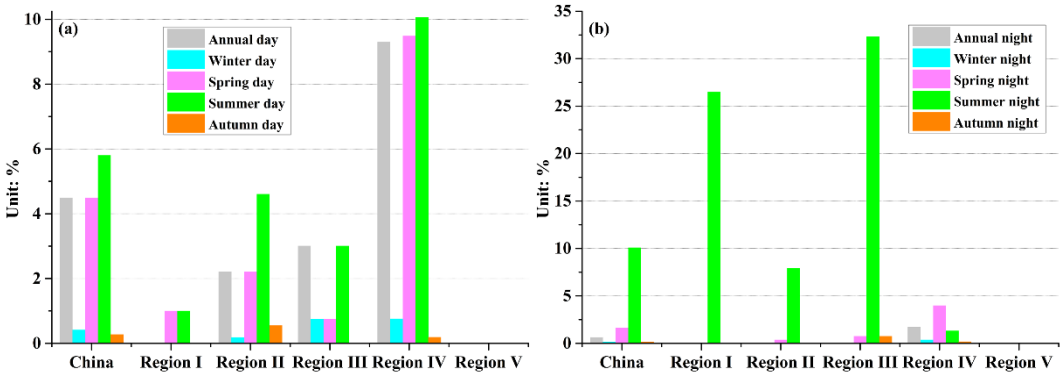

Figure S4. The percentages of urban regions whose annual and seasonal variation rates of mean LSTs significantly positively changed during both the daytime and night-time from 2003 to 2013 in the five environmental regions of China.

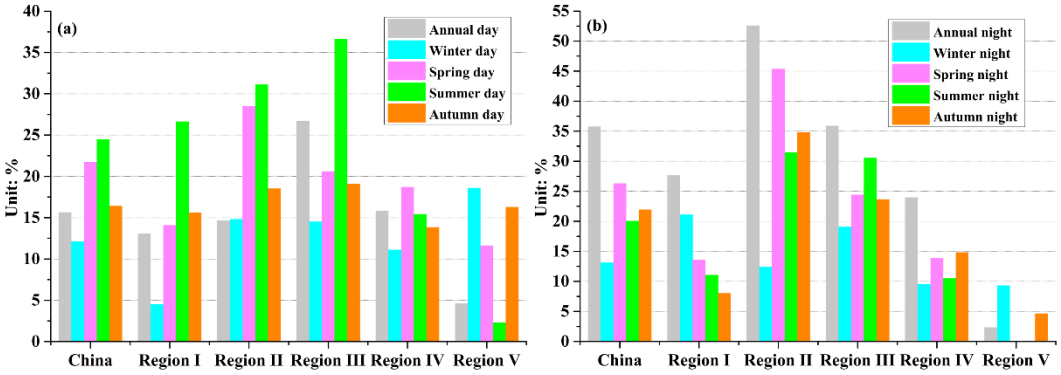

Figure S5. The percentages of cities whose annual and seasonal variation rates of mean SUHIIs significantly changed during both the daytime and night-time from 2003 to 2013 in the five environmental regions of China.

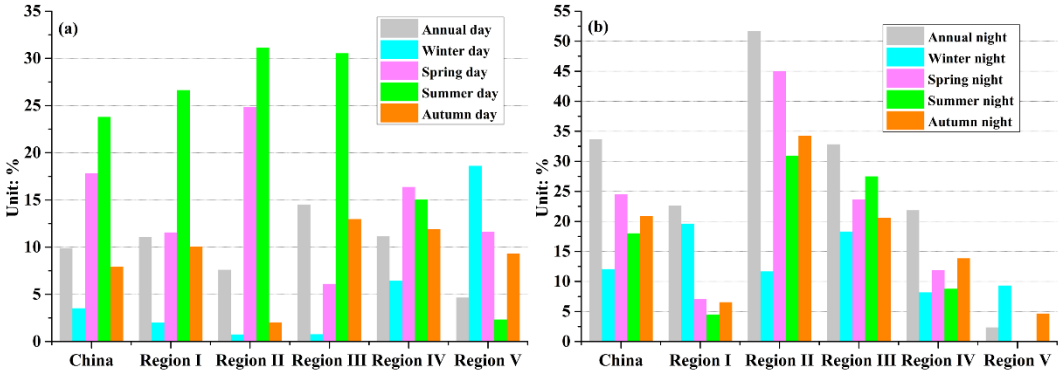

Figure S6. The percentages of cities whose annual and seasonal variation rates of mean SUHIIs significantly positively changed during the daytime and night-time, and differences between the daytime and night-time rates from 2003 to 2013 in the five environmental regions of China.

Supporting table

Table S1. Typical monitoring indicators of SUHIIs.

Type	Indicator	Units	Quantification in this study	Sensor; temporal resolution; study area
Land cover types driven	Difference urban core − rural	K	Difference in mean LST between urban cores (pixels having 75% to 100% impervious surface area (ISA)) and rural areas (pixels located in a 5 km wide ring located between 45 and 50, or 15 and 20 km away from the 25% ISA contour and having less than 5% ISA)	MODIS; day and night; several days; American continental mega cities; (Imhoff *et al.*, 2010)
				MODIS; day and night; several years; more than 3000 cities in global; (Zhang *et al.*, 2010)
	Difference urban−rural	K	Difference in mean LST between urban areas (derived by aggregating regions with ISA > 50%) and rural areas (the farthest three buffer zones in 12 zones with a half of area of the city)	MODIS; day and night; several years; 32 large cities in China; (Zhou *et al.*, 2015)
		K	Difference in mean LST between urban areas (derived by aggregating regions with ISA > 50%) and rural areas (pixels located in a 5 km wide ring located between 45 and 50 km away from urban areas, excluding pixels of waterbodies and with elevation of 50 m larger than the maximum value in urban area)	MODIS; day and night; several years; 32 large cities in China; (Zhou *et al.*, 2016)
		K	Difference in mean LST between urban areas (4-connected pixel clusters of multi-story structure cities) and rural areas (pixels located in a 5 km wide ring located between 45 and 50 km away from urban areas, excluding pixels of waterbodies and urban regions)	MODIS; day and night; one years; 193090 cities in global; (Clinton and Gong, 2013)
		K	Difference in mean LST between pixels in which the urban and rural weather observation stations locate	MODIS; day and night; summer in several years; Birmingham; (Tomlinson *et al.*, 2012)
	Difference urban core − outskirt	K	Difference in mean LST between urban cores (regions composed by 3×3 pure pixels inside urban region) and suburban areas (four 3×3 pixels located in four directions of urban cores with mean elevation differences of 100 m less than them in corresponding urban cores)	MODIS; day and night; several years; 39 large cities in China; (Cao *et al.*, 2016)
	Difference urban core − outskirt	K	Difference in mean LST between urban cores (regions derived by cluster algorithm) and suburban areas (buffer zones surrounding urban areas with the same area, not including waterbodies pixels)	MODIS; day and night; several years; 419 large cities in global; (Peng *et al.*, 2011)
			Difference in mean LST between urban cores (regions derived by aggregating regions with ISA > 50%) and suburban areas (buffer zones surrounding urban areas with the same area, not including waterbodies pixels)	MODIS; day and night; several years; 32 large cities in China; (Zhou *et al.*, 2014)
	Difference urban−agriculture	K	Difference in mean LST between urban area and cropland	MODIS; day and night, several days; global observation; (Jin *et al.*, 2005)
				MODIS; day and night, 2 years; Teheran; (Haashemi *et al.*, 2016)

	Difference urban−forest	K	Difference in mean LST between urban area and forest	MODIS; day and night, several days; global observation; (Jin *et al.*, 2005)
			Difference in mean LST between urban area (continuous areas dominated by high density built-up land (> 50%) & less than two kilometers away from the perimeter of water body were excluded) and forest (estimated from natural forest LSTs wall-to-wall by a simple planar surface model)	MODIS; day and night, several years; Yangtze River Delta Urban Agglomeration; (Zhou *et al.*, 2018)
	Difference uran-water	℃	Difference in mean LST between urban area and water surface	Landsat-TM and ETM++; several days; the Pearl River Delta; (Zhang *et al.*, 2006)
				MODIS; day and night, 2 years; Teheran; (Haashemi *et al.*, 2016)
	Difference urban−other	K	Difference in mean LST between urban area and outskirts or coastal areas	NOAA-AVHRR; day and night; several days; Los Angeles; (Dousset and Gourmelon, 2003)
	Micro-UHI	%	Percentage of areas (without water surfaces) with LST higher than the warmest LST associated with tree canopies	Landsat-TM; 1 image; a portion of Dallas, Texas; (Aniello *et al.*, 1995)
LST pattern driven	Gaussian area	km^2	Areas under a Gaussian surface fitted to LST, after the rural LST background has been subtracted	NOAA-AVHRR; night, several days, Houston; (Streutker, 2002; Streutker, 2003)
				MODIS; day and night, several days; Asian mega cities; (Tran *et al.*, 2006)
	Gaussian magnitude	K	Maximum of a Gaussian surface fitted to LST, after the rural LST background has been subtracted	NOAA-AVHRR; night, several days; Houston; (Streutker, 2003)
				MODIS; day and night, several days; Asian mega cities; (Tran *et al.*, 2006)
	Gaussian magnitude empirical	K	Maximum difference between the temperatures in urban and fitted rural temperature surfaces	MODIS; several days; European cities; (Schwarz *et al.*, 2011)
	Standard deviation	Null	The standard deviation of the LST in a city	MODIS; several days; European cities; (Schwarz *et al.*, 2011)
	Magnitude	K	Difference between maximum and mean of LST	MODIS; day and night, several days; Indianapolis; (Rajasekar and Weng, 2009)
	Hot island area derived by mathematical statistics of LST	km^2	Area with LST higher than the mean plus one standard deviation	Landsat-ETM++; 1 image; ten cities in Guangdong; (Zhang and Wang, 2008)
	Difference high – low	℃	Difference in mean LST between high LST (>mean+1*sd) area and low LST (<mean-1*sd) area	Landsat TM and ETM+; several days; The Pearl River Delta; (Zhang, 2006)
	Urban thermal field variance index	null	Ratio of difference of LST in each pixel and mean value in this region and mean value in this region	CBERS02-IRMSS; daytime, one day; Beijing, Wuxi; (Zhang *et al.*, 2006)
	Hot island area derived by spatial statistics of LST	km^2	Identify clusters of high and low LST using spatial correlation based on Moran index and statistics based on hotspot analysis	Landsat Landsat/TM、ETM+; day, four days in four years; Hangzhou; (Zhang *et al.*, 2015)

	Hot island area derived by detecting abrupt changes	km^2 & ℃	Use Rodionov test to identify shifting points between in profiles of LST; obtain influence regions of SUHI; calculate difference between mean LST in above-mentioned regions and their buffer zones with buffer distances of 5 and 10 km, respectively	MODIS; day and night, July in several years; Bucharest; (Cheval and Dumitrescu, 2009)
	Brightness - temperature - grade - change - index (TGCI)	null	Make separate level division for two period images; and synthetically considerate level degree change type and all type proportion, aiming to analyze UHI intensity trends	Landsat-TM and ETM+;day; two images for two years； Xiamen; (Xu *et al.*, 2011)
Complex driven by land cover type and LST pattern	Urban - heat - island - ratio - index (URI)	null	Synthetically considerate level proportion and degree with LST higher than suburban area; and give a value between 0 and 1	Landsat-TM and ETM+; day; several days; Xiamen; (Xu and Chen, 2003)
	Weighted - average - heat - island - intensity (WAI)	℃	Synthetically considerate level proportion and difference to mean LST in study area for all levels	Landsat-TM and ETM+; day; Nanchong and Guang'an; (Dan *et al.*, 2010)

References

Aniello C, Morgan K, Busbey A, Newland L. 1995. Mapping micro-urban heat islands using Landsat TM and a GIS. *Computers & Geosciences* **21**: 965-969. doi: 10.1016/0098-3004(95)00033-5.

Cao C, Lee X, Liu S, Schultz N, Xiao W, Zhang M, Zhao L. 2016. Urban heat islands in China enhanced by haze pollution. *Nature Communications* **7**: 12509. doi:10.1038/ncomms12509.

Cheval S, Dumitrescu A. 2009. The July urban heat island of Bucharest as derived from modis images. *Theoretical and Applied Climatology* **96**: 145-153. doi:10.1007/s00704-008-0019-3.

Clinton N, Gong P. 2013. MODIS detected surface urban heat islands and sinks: Global locations and controls. *Remote Sensing of Environment* **134**: 294-304. doi:10.1016/j.rse.2013.03.008.

Dan S, Xu H, Xue W, He J, Dan B. 2010. Comparison and analysis of research methods for urban heat island effect based on Landsat TM6. Pages 161-164 *in* Geoscience and Remote Sensing (IITA-GRS), 2010 Second IITA International Conference on. IEEE.

Dousset B, Gourmelon F. 2003. Satellite multi-sensor data analysis of urban surface temperatures and landcover. *ISPRS Journal of Photogrammetry and Remote Sensing* **58**: 43-54. doi:10.1016/s0924-2716(03)00016-9.

Haashemi S, Weng Q, Darvishi A, Alavipanah SK. 2016. Seasonal variations of the surface urban heat island in a semi-arid city. *Remote Sensing* **8**: 352. doi: 10.3390/rs8040352.

Imhoff ML, Zhang P, Wolfe RE, Bounoua L. 2010. Remote sensing of the urban heat island effect across biomes in the continental USA. *Remote Sensing of Environment* **114**: 504-513. doi:10.1016/j.rse.2009.10.008.

Jin M, Dickinson RE, Zhang D. 2005. The footprint of urban areas on global climate as characterized by MODIS. *Journal of Climate* **18**: 1551-1565. doi: 10.1175/jcli3334.1.

Peng S, Piao S, Ciais P, Friedlingstein P, Ottle C, Bréon FO-M, Nan H, Zhou L, Myneni RB. 2011. Surface urban heat island across 419 global big cities. *Environmental science & technology* **46**: 696-703. doi: 10.1021/es2030438.

Rajasekar U, Weng Q. 2009. Urban heat island monitoring and analysis using a non-parametric model: A case study of Indianapolis. *ISPRS Journal of Photogrammetry and Remote Sensing* **64**: 86-96. doi:10.1016/j.isprsjprs.2008.05.002.

Schwarz N, Lautenbach S, Seppelt R. 2011. Exploring indicators for quantifying surface urban heat islands of European cities with MODIS land surface temperatures. *Remote Sensing of Environment* **115**: 3175-3186. doi:10.1016/j.rse.2011.07.003.

Streutker DR. 2002. A remote sensing study of the urban heat island of Houston, Texas. *International Journal of Remote Sensing* **23**: 2595-2608. doi:10.1080/01431160110115023.

Streutker DR. 2003. Satellite-measured growth of the urban heat island of Houston, Texas. *Remote*

Sensing of Environment **85**: 282-289. doi: 10.1016/S0034-4257(03)00007-5.
Tomlinson CJ, Chapman L, Thornes JE, Baker CJ. 2012. Derivation of Birmingham's summer surface urban heat island from MODIS satellite images. *International Journal of Climatology* **32**: 214–224. doi: 10.1002/joc.2261.
Tran H, Uchihama D, Ochi S, Yasuoka Y. 2006. Assessment with satellite data of the urban heat island effects in Asian mega cities. *International Journal of Applied Earth Observation and Geoinformation* **8**: 34-48. doi:10.1016/j.jag.2005.05.003.
Xu H, Chen B. 2003. An image processing technique for the study of urban heat island changes using different seasonal remote sensing data. *Remote Sensing Technology and Application* **18**: 129-133. doi: 10.3969/j.issn.1004-0323.2003.03.002
Xu H, Chen Y, Dan S, Qiu W. 2011. Dynamical monitoring and evaluation methods to urban heat island effects based on RS & GIS. *Procedia Environmental Sciences* **10**: 1228-1237. doi:10.1016/j.proenv.2011.09.197.
Zhang J. 2006. Thermal environment detection in the Pearl River Delta area by remote sensing and analysis of its
spatial and temporal evolutions. Graduate University of Chinese Academy of Sciences, Guangzhou.
Zhang J, Wang Y. 2008. Study of the relationships between the spatial extent of surface urban heat islands and urban characteristic factors based on Landsat ETM+ data. *Sensors* **8**: 7453-7468. doi: 10.3390/s8117453.
Zhang P, Imhoff ML, Wolfe RE, Bounoua L. 2010. Characterizing urban heat islands of global settlements using MODIS and nighttime lights products. *Canadian Journal of Remote Sensing* **36**: 185-196. doi:10.5589/m10-039.
Zhang W, Jiang J, Zhu Y. 2015. Spatial-temporal evolution of urban thermal environment based on spatial statistical features. *Chinese Journal of Applied Ecology* **26**: 1840-1846. doi:10.13287/j.1001-9332.20150331.003.
Zhang Y, Yu T, Gu X, Zhang Y, Chen L, Yu S, Li W, Li X. 2006. Land surface temperature retrieval from CBERS-02 IRMSS thermal infrared data and its applications in quantitative analysis of urban heat island effect. *Journal of Remote Sensing*: 789-797. doi: 10.1016/S0379-4172(06)60102-9.
Zhou D, Bonafoni S, Zhang L, Wang R. 2018. Remote sensing of the urban heat island effect in a highly populated urban agglomeration area in East China. *Science of the Total Environment* **s 628–629**: 415-429. doi: 10.1016/j.scitotenv.2018.02.074.
Zhou D, Zhang L, Li D, Huang D, Zhu C. 2016. Climate–vegetation control on the diurnal and seasonal variations of surface urban heat islands in China. *Environmental Research Letters* **11**: 074009. doi:10.1088/1748-9326/11/7/074009.
Zhou D, Zhao S, Liu S, Zhang L, Chao Z. 2014. Surface urban heat island in China's 32 major cities: Spatial patterns and drivers. *Remote Sensing of Environment* **152**: 51-61. doi:10.1016/j.rse.2014.05.017.
Zhou D, Zhao S, Zhang L, Sun G, Liu Y. 2015. The footprint of urban heat island effect in China. *Scientific Reports* **5**: 11160. doi: 10.1038/srep11160.